Astronomical Techniques and Instruments, Vol. 3, May 2026, 1–10

Article Open Access

# A horizontal limit avoidance strategy for the equatorial telescope pointing process

**Xiaoyan Li[1,2*], Yuling Cai[1,2,3], Yanbing Chen[1,2,3]**

[1]*Nanjing Institute of Astronomical Optics & Technology*, *Chinese Academy of Sciences*, *Nanjing* 210042, *China*

[2]*CAS Key Laboratory of Astronomical Optics & Technology*, *Nanjing Institute of Astronomical Optics & Technology*, *Nanjing* 210042, *China*

[3]*University of Chinese Academy of Sciences*, *Beijing* 100049, *China*

*Correspondence: xyli@niaot.ac.cn

Received: July 22, 2025; Accepted: August 15, 2025; Published Online: August 16, 2025; https://doi.org/10.3724/ati2025064; https://cstr.cn/32083.14.ati2025064

© 2026 Editorial Office of Astronomical Techniques and Instruments, Yunnan Observatories, Chinese Academy of Sciences. This is an open access article under the CC BY 4.0 license (http://creativecommons.org/licenses/by/4.0/)

Citation: Li, X. Y., Cai, Y. L., Chen, Y. B. 2026. A horizontal limit avoidance strategy for the equatorial telescope pointing process. *Astronomical Techniques and Instruments*, **3**(3): 1−10. https://doi.org/10.3724/ati2025064.

**Abstract:** Time-domain astronomy requires telescopes capable of rapid response and uninterrupted operation to observe light curves of transient astrophysical events in the shortest possible time. For equatorial telescopes, which are mainly used for meter-class telescopes, it is possible for the horizontal limit stop to interrupt the observation, especially during the pointing process as the telescope slews to the next object to observe. We discuss the procedures to estimate whether the horizontal limit stop will occur in the pointing process and propose an algorithm to prevent this. We consider several factors relating to the horizontal limit stop, including the latitude of the observation site, the current pointing of the telescope, the target pointing, the degree threshold of the horizontal limit stop, and the altitude threshold of the observable sky area for astronomy. Once factors are given, a set of discrimination procedures is conducted to determine whether the horizontal limit stop will be triggered in a single pointing process. If it is predicted to occur, then the telescope control software will alter the pointing course. Finally, we discuss some other related factors, such as RA and DEC axes having different pointing speeds, and observation sites in the Southern Hemisphere We demonstrate a method to keep equatorial astronomical telescopes away from the horizontal limit stop while in motion. This system can be beneficial if operating continuously for autonomous observations, to guarantee a rapid response for time-domain astronomy.

**Keywords:** Equatorial telescope; Horizontal limit stop; Limit prevention; Algorithm; Telescope control software

## 1. INTRODUCTION

An equatorially mounted telescope can compensate for Earth's rotation by having one rotational axis (the right ascension or polar axis) parallel to the Earth's axis of rotation. The advantage of an equatorial mount lies in its ability to allow the instrument attached to it to stay fixed on any celestial object with diurnal motion by driving one axis at a constant speed[1,2]. In addition, for astrophotography, the image does not rotate in the focal plane, as occurs with altazimuth mounts when they are tracking the target's motion, unless a field-derotator is installed. Consequently, equatorial mounts are widely used for small and medium-sized telescopes.

Modern reflector telescopes, with mid- to large-sized apertures, should never be tilted close to the horizon, because the large primary mirrors are usually not firmly fixed to the telescope frame but left floating inside a mechanical cell. The primary mirror support system of a telescope typically consists of an axial support and edge-lateral support[3]. This enables premium-quality mirrors to capture optical images free from any distortions caused by bolting the mirror onto the framework[4,5]. However, this makes the primary mirror highly vulnerable to accidental damage, degraded image quality caused by mirror misalignment, or incidents of the mirror completely falling out of the apparatus. Equatorial telescopes have a coordination difference compared with altazimuthal mounts, which makes it impossible to prevent excessive low-tilt using only mechanical limit stops. They must therefore be equipped with tilt sensors, like mercury tilt switches or opto-mechanical devices[6]. When the tube is close to the horizontal position, tilt sensors will trigger a limit stop signal and halt the telescope, to protect the primary mirror.

Time-domain survey telescopes are primarily used to observe light curves of transient astrophysical events,

which exhibit their most critical early-time evolution within a few hours or less, in the shortest possible time[7,8]. Capturing these changes requires telescopes capable of rapid response and uninterrupted operation, typically with automatic or autonomous operation[9], so it is useful to study how to avoid the horizontal tilt limit stop for equatorial telescopes, especially time-domain surveyors.

The process by which a telescope observes an object can be typically divided into two stages: pointing and tracking. Pointing is a higher-speed slewing stage of motion of the two axes of the telescope, from the current position to the target position, while tracking is a lower-speed rotation stage when the telescope acquires an image of the object and follows its motion across the sky. In most cases, when astronomers make an observation schedule, they can easily find the object altitude during the observation time and avoid the horizontal limit stop during tracking stage. In this paper, we focus on the pointing stage in which it is easier to trigger the horizontal limit stop. In addition, for most cases, we limit the readings of the two axes to within the range of the polar axis as [−180°, 180°] and the declination (DEC) axis as [−90°, 90°], which may be beyond the range of some telescopes.

In Section 2, we discuss the trajectory of the telescope tube orientation in the pointing process on a two-dimensional chart, using hour angle (HA) and DEC as the coordinate system. We then discuss several factors relating to the horizontal limit stop, followed by procedures to estimate whether the limit stop will be triggered. Section 3 gives a method to prevent the limit stop by altering the pointing course. Section 4 combines the procedures in the previous two sections into an entire workflow. Section 5 gives an extended discussion by altering some conditions, such as different axes and slew speed. Our conclusions are presented in Section 6.

## 2. PREDICTION PROCEDURES

After unfolding the equatorial celestial coordinate system, using a method similar to the orthographic cylindrical projection, we can obtain a plane diagram with HA as the horizontal coordinate and DEC as the vertical coordinate, on which we can plot contour lines of tube orientation altitude. As shown in Fig. 1, when the geographical latitude ($\varphi$) of the observatory site is 70°, contour lines of altitudes 0° and 10° divide the HA-DEC plane into three regions: the first has altitude greater than 10°, the second is between 0° and 10°, and the third is less than 0°.

The pointing trajectory of the telescope can be graphically represented using lines. We assume that the two axes have the same maximum pointing speed and acceleration, which is typical of most telescopes. The pointing trajectory on the diagram is represented by a line segment with a slope approximately 1 or −1 when slewing on both axes. Subsequently, when one axis reaches the target position, the speed slows and the telescope enters tracking mode, while the other axis continues to slew at pointing

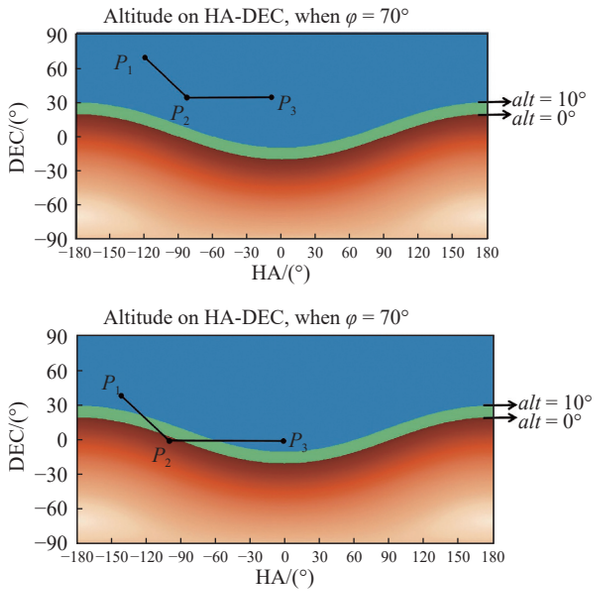


**Fig. 1. HA-DEC plane diagram with lines showing the trajectory of the telescope pointing process.**

speed. At this stage, the trajectory on the chart is shown by an approximately horizontal or vertical line segment. Section 5 will discuss instances in which the maximum pointing speeds of the two axes are not consistent.

We assume the current position of the telescope to be point $P_1(P_{1H}, P_{1D})$, and the target position is point $P_3$ $(P_{3H}, P_{3D})$. As shown in Fig. 1, the movement trajectory follows a path of $P_1$–$P_2$–$P_3$, where $P_2$ is the turning point of the dual-axis and single-axis pointing process. As the upper panel of Fig. 1 shows, the limit stop will not be triggered if the pointing path never passes the third region, while the lower panel shows the telescope will pass below horizontal and trigger the limit stop.

During the pointing process, several factors determine whether the horizontal limit stop will be triggered. These include the latitude of the observation site ($\varphi$), the current position $P_1(P_{1H}, P_{1D})$ and target position $P_3(P_{3H}, P_{3D})$ of the telescope axes, the horizontal limit stop threshold ($T_0$), and the lower altitude threshold of the observable sky area for astronomy ($T_1$).

$T_0$ is generally greater than or equal to 0°, set by the telescope manufacturer to ensure the safety of the primary mirror. $T_1$ is typically set by the telescope operators depending on the requirements of the observation being undertaken. For example, in stellar astronomy, stars with altitude above 30° are typically observed, to avoid light pollution or telluric contamination associated with high airmass along the sightline. For observations of satellites, which are typically bright, the required observable range is just above 0°. Generally, $T_1$ is often set to be greater than $T_0$, i.e., the minimum altitude of the observable sky area should be greater than the horizontal limit stop. In the following subsections, we discuss these factors for observation sites in the Northern Hemisphere. An analysis for sites in the Southern Hemisphere will be provided in Section 5.

### 2.1. $T_1$—the Altitude Threshold of the Observable Sky Area for Astronomy

For an observation site with a latitude of 25°, as an example, Fig. 2 shows the differences between $T_0$ and $T_1$ for two cases: $T_0 = 0°$ and $T_1 = 15°$, and $T_0 = 0°$ and $T_1 = 35°$. When $T_1 = 35°$, the observable region has a convex geometry, which means that for each pair of points within the region, every point on the line segment connecting the two points also lies within the region[10]. In other words, when the telescope moves between any two points, the path will not be outside the observable region. However, when $T_1 = 15°$, the observable region is a concave one, that means at least one line segment between two points in the region passes outside the region. Therefore, we must discuss it in two cases: the region is a convex, and the region is a concave.

The critical point deciding the region is convex or concave is the intersection point of the $T_1$ contour line and the line at $DEC = 90°$. The $T_1$ contour lines can be found using the relation

$$\sin T_1 = \sin\varphi \sin DEC + \cos\varphi \cos HA \cos DEC, \qquad (1)$$

when $DEC = 90°$, $\sin T_1 = \sin\varphi$. where $\varphi$ is the latitude of the observation site.

When $T_1 \geqslant \varphi$, i.e., when the lower altitude of the observable sky area $T_1$ is greater than the latitude of the observation site $\varphi$, the observable region is convex. Within this region, the horizontal limit stop will not be triggered. Otherwise, further analysis is required.

### 2.2. $\varphi$–Latitude of the Observation Site

Assuming the horizontal limit stop, $T_0$, and the observable altitude threshold, $T_1$, are set to 0° and 15°, respectively, the $T_0$ and $T_1$ contour lines are plotted for different observation site latitudes $\varphi$, such as 25°, 40°, 55°, and 70° in Fig. 3. The maximum slope of the $T_0$ contour line varies with the observation site latitude. The higher the latitude $\varphi$ is, the smaller the maximum absolute value of the slopes. As mentioned previously, the trajectory of the telescope during the pointing process is a line segment with a slope approximately equal to 1 or −1. Therefore, the discussion is divided into two cases based on whether the maximum slope of the $T_0$ contour line exceeds 1.

In Equation (1), it is assumed that $DEC \neq \pm 90°$, i.e., $\cos DEC \neq 0$. After dividing both sides by $\cos DEC$ and

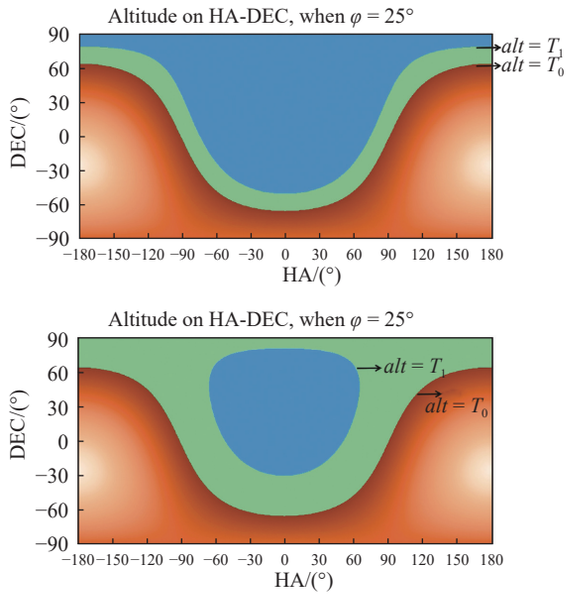


**Fig. 2. At a latitude of 25°, the upper chart shows that when $T_1$ = 15° there is no convex region in the observable region (blue), while the lower chart shows that when $T_1$ = 25° a convex region exists in the observable region (blue).**

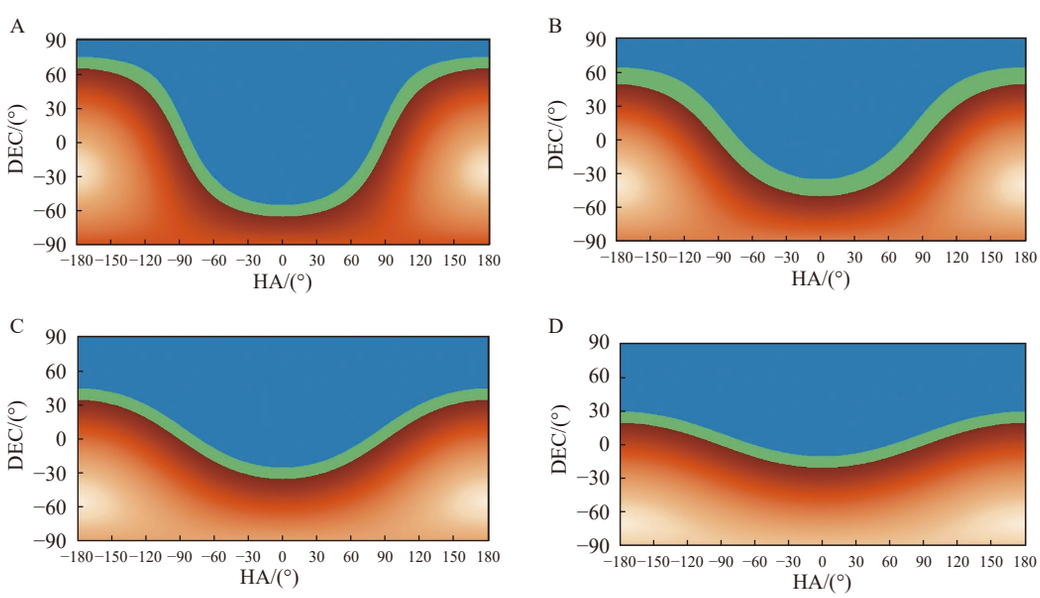


**Fig. 3. Observable regions at different observation site latitudes, altitude on HA-DEC.** (A) $\varphi$ = 25°. (B) $\varphi$ = 40°. (C) $\varphi$ = 55°. (D) $\varphi$ = 70°.

taking the derivative of $HA$, Equation (2) is derived as

$$\sec^2 DEC \frac{\mathrm{d}DEC}{\mathrm{d}HA} = \cot\varphi \sin HA. \tag{2}$$

When the slope of the $T_0$ contour line is less than 1, $|\mathrm{d}DEC/\mathrm{d}HA| < 1$, we find

$$\left|\cot\varphi \sin HA \cos^2 DEC\right| < 1. \tag{3}$$

Because the observation site latitude $\varphi \in (0°, 90°)$, $\cot\varphi > 0$, and $\cos^2 DEC \leqslant 1$, we find

$$\cot\varphi |\sin HA| \cos^2 DEC < 1. \tag{4}$$

The value range of $HA$ is $[-180°, 180°]$, and that of $DEC$ is $(-90°, 90°)$, so the condition $\cot\varphi < 1$ must be met for Equation (4) to hold true. This means that when $\varphi > 45°$, the absolute value of the slopes of the $T_0$ contour line are all less than 1.

So we will discuss the following two cases:

$\varphi \leqslant 45°$: The maximum slope of the $T_0$ contour is greater than or equal to 1;

$\varphi > 45°$: The absolute value of the slopes of the $T_0$ contour are all less than 1.

### 2.2.1. $\varphi \leqslant 45°$

Taking $\varphi = 15°$, 25°, and 45° as examples, the two tangents with slopes of 1 and −1 are drawn on the $T_0$ contour line, with the intersection points as $C_1(C_{1H}, C_{1D})$ and $C_2(C_{2H}, C_{2D})$. These two tangents divide the area above the $T_0$ contour line into regions $A$, $B_1$, $B_2$, and $B_3$, as shown in Fig. 4, representing three different typical cases.

The process for determining which region ($A$, $B_1$, $B_2$, or $B_3$) the telescope's current position $P_1$ and the target position $P_3$ falls into is as follows:

Step 1: Find the coordinates of the intersection points $C_1$ and $C_2$.

Based on the transformation formula between the equatorial and horizontal coordinate systems, substitute the coordinates of the intersection point $C_1(C_{1H}, C_{1D})$ into the $T_0$ contour equation,

$$\sin T_0 = \sin\varphi \sin C_{1D} + \cos\varphi \cos C_{1D} \cos C_{1H}. \tag{5}$$

Next, by differentiating Equation (1) and substituting the slope value −1, we obtain

$$0 = \cos C_{1D} \sin\varphi - \sin C_{1D} \cos C_{1H} \cos\varphi + \cos C_{1D} \sin C_{1H} \cos\varphi. \tag{6}$$

Similarly, substituting the slope value 1 leads to

$$0 = \cos C_{1D} \sin\varphi + \sin C_{1D} \cos C_{1H} \cos\varphi + \cos C_{1D} \sin C_{1H} \cos\varphi. \tag{7}$$

Finally, the coordinates of $C_1$ are determined by solving Equation (5) and Equation (6), while $C_2$ is obtained by solving Equation (5) and Equation (7).

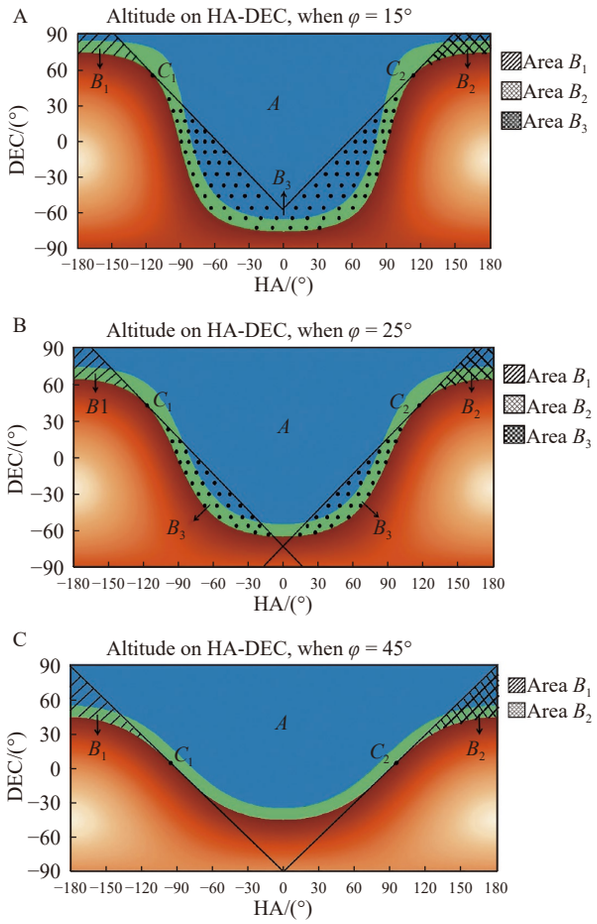


**Fig. 4. When the latitude of the observation site is 15° (A), 25° (B) and 45° (C), lines with slopes of 1 and −1 divide the areas above the $T_0$ contour into the regions, $A$, $B_1$, $B_2$, and $B_3$.**

Using the fsolve function in the Python SciPy package, solve the nonlinear system of equations and obtain the coordinates of $C_1$ and $C_2$.

```
1. procedure EQUATIONS (vars, T0, φ)
2.     x,y = vars
3.     eq1 = sinT0 − (sinφ sin y + cosφ cos y cos x)
4.     eq2 = sinφ cos y − cosφ sin y cos x + cosφ cos y sin x
5.     return [eq1, eq2]
6. end procedure
7.     Solve the system of equations
8. solution = fsolve(equations, initial_guess, args = (T0, φ))
```

Step 2: For the tangent line which passing through points $C_1$ and $C_2$, derive

$$\begin{aligned} l_{C_1} &: X_D + X_H - C_{1H} - C_{1D} = 0, \\ l_{C_2} &: X_D - X_H + C_{2H} - C_{2D} = 0. \end{aligned} \tag{8}$$

Step 3: Use the above tangent line equations to determine which region $A$, $B_1$, $B_2$, or $B_3$ a certain point $P(P_H, P_D)$ belongs to:

When $P_H \in (-180°, C_{1H})$, $P_D + P_H - C_{1H} - C_{1D} > 0$; $P \in A$; Otherwise, $P \in B_1$;

When $P_H \in (C_{1H}, 0)$, $P_D + P_H - C_{1H} - C_{1D} > 0; P \in A$; Otherwise, $P \in B_3$;

When $P_H \in (0, C_{2H})$, $P_D - P_H + C_{2H} - C_{2D} > 0$; $P \in A$; Otherwise, $P \in B_3$;

When $P_H \in (C_{2H}, 180°)$, $P_D - P_H + C_{2H} - C_{2D} > 0$; $P \in A$; Otherwise, $P \in B_2$.

When $P_1$ and $P_3$ fall into different regions, there are 16 possibilities for the pointing process, as shown in Table 1.

**Table 1. Possibilities for the pointing process**

| Current position $P_1$ | Target position $P_3$ | | | |
|---|---|---|---|---|
| | $A$ | $B_1$ | $B_2$ | $B_3$ |
| $A$ | $A \to A$ | $A \to B_1$ | $A \to B_2$ | $A \to B_3$ |
| $B_1$ | $B_1 \to A$ | $B_1 \to B_1$ | $B_1 \to B_2$ | $B_1 \to B_3$ |
| $B_2$ | $B_2 \to A$ | $B_2 \to B_1$ | $B_2 \to B_2$ | $B_2 \to B_3$ |
| $B_3$ | $B_3 \to A$ | $B_3 \to B_1$ | $B_3 \to B_2$ | $B_3 \to B_3$ |

Meanwhile, the relative positions of points $P_1$ and $P_3$ determine the pattern of the pointing trajectory, i.e., the permutations and combinations of $P_{1H} > P_{3H}$, $P_{1H} < P_{3H}$, $P_{1H} = P_{3H}$ with $P_{1D} > P_{3D}$, $P_{1D} < P_{3D}$, $P_{1D} = P_{3D}$, as well as $|P_{1H} - P_{3H}| > |P_{1D} - P_{3D}|$, $|P_{1H} - P_{3H}| < |P_{1D} - P_{3D}|$, $|P_{1H} - P_{3H}| = |P_{1D} - P_{3D}|$, as shown in the Table 2.

**Table 2. 16 types of trajectory shapes during the pointing process**

| | $P_{1D} > P_{3D}$ | | | $P_{1D} < P_{3D}$ | | | $P_{1D} = P_{3D}$ |
|---|---|---|---|---|---|---|---|
| | $\lvert P_{1H} - P_{3H}\rvert > \lvert P_{1D} - P_{3D}\rvert$ | $\lvert P_{1H} - P_{3H}\rvert < \lvert P_{1D} - P_{3D}\rvert$ | $\lvert P_{1H} - P_{3H}\rvert = \lvert P_{1D} - P_{3D}\rvert$ | $\lvert P_{1H} - P_{3H}\rvert > \lvert P_{1D} - P_{3D}\rvert$ | $\lvert P_{1H} - P_{3H}\rvert < \lvert P_{1D} - P_{3D}\rvert$ | $\lvert P_{1H} - P_{3H}\rvert = \lvert P_{1D} - P_{3D}\rvert$ | |
| $P_{1H} > P_{3H}$ | 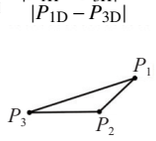 | 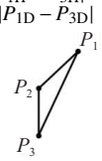 | 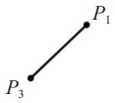 | 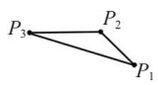 | 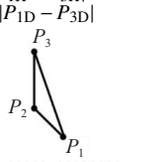 | 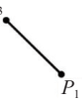 |  |
| $P_{1H} < P_{3H}$ | 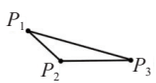 | 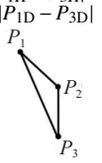 | 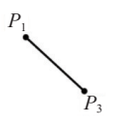 | 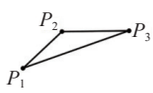 | 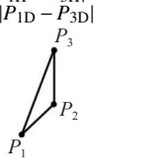 | 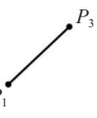 |  |
| $P_{1H} = P_{3H}$ |  | | |  | | | |

Table 3 shows what will happen when $P_1$ and $P_3$ belong to different regions, in which the "×" symbol indicates the horizontal limit stop will be triggered, the "◦" symbol indicates that it will not, and the "?" symbol indicates that further analysis is needed, which is shown as:

**Table 3. Horizontal limit stop trigger vs. Regions that $P_1$ and $P_3$ belongs to (× will trigger, ◦ will not, ? is uncertain.)**

| $P_1$ | $P_3$ | | | |
|---|---|---|---|---|
| | $A$ | $B_1$ | $B_2$ | $B_3$ |
| $A$ | ◦ | ◦ | ◦ | ◦ |
| $B_1$ | ? | ◦ | ◦ | × |
| $B_2$ | ? | ◦ | ◦ | × |
| $B_3$ | ? | ? | ? | ◦ |

The first step involves obtaining the coordination of turning point $P_2$. Depending on the relative positions of $P_1$ and $P_3$, the equations for calculating $P_{2H}$ and $P_{2D}$ are as follows:

When $\|P_{1H} - P_{3H}\| > \|P_{1D} - P_{3D}\|$ and $\dfrac{P_{1D} - P_{3D}}{P_{1H} - P_{3H}} < -1$, the coordinates are calculated as:

$$P_{2D} = P_{3D}, \tag{9}$$

$$P_{2H} = P_{1D} - P_{3D} + P_{1H}. \tag{10}$$

When $\|P_{1H} - P_{3H}\| < \|P_{1D} - P_{3D}\|$ and $\dfrac{P_{1D} - P_{3D}}{P_{1H} - P_{3H}} > -1$, the coordinates become:

$$P_{2H} = P_{3H}, \tag{11}$$

$$P_{2D} = P_{1H} - P_{3H} + P_{1D}. \tag{12}$$

For the case where $\|P_{1H} - P_{3H}\| > \|P_{1D} - P_{3D}\|$ and $\dfrac{P_{1D} - P_{3D}}{P_{1H} - P_{3H}} < 1$, the equations are:

$$P_{2D} = P_{3D}, \tag{13}$$

$$P_{2H} = P_{3D} - P_{1D} + P_{1H}. \tag{14}$$

Finally, when $\|P_{1H} - P_{3H}\| < \|P_{1D} - P_{3D}\|$ and $\dfrac{P_{1D} - P_{3D}}{P_{1H} - P_{3H}} > 1$, the coordinates are given by:

$$P_{2H} = P_{3H}, \tag{15}$$

$$P_{2D} = P_{3H} - P_{1H} + P_{1D}. \quad (16)$$

The next step is determining whether $P_2$ is below the horizontal limit. Substitute $P_{2H}$ and $P_{2D}$ into the altitude equation,

$$\sin ALT_{P_2} = \sin P_{2D} \sin\varphi + \cos P_{2D} \cos P_{2H} \cos\varphi, \quad (17)$$

to obtain the altitude angle of point $P_2$, denoted as $ALT_{P_2}$. If $ALT_{P_2} < T_0$. The altitude of point $P_2$ is lower than the horizontal limit stop altitude $T_0$, indicating that the limit stop will be definitely triggered in the pointing process.

If $ALT_{P_2} > T_0$, it is necessary to further determine the regions to which $P_1$ and $P_2$ belong, as shown in Fig. 5. If $P_1 \in B_1$ or $B_2$, and $P_2 \in B_3$, the horizontal limit stop will be triggered when the pointing process passes through the area below the horizontal.

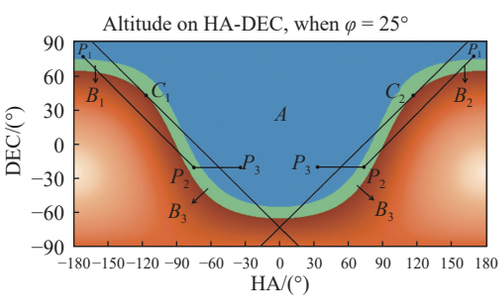


**Fig. 5. When $P_1$ is located at the $B_1$ or $B_2$ region and $P_2$ belongs to the $B_3$ region, the horizontal limit stop will be triggered, even if $ALT_{P_2} > T_0$.**

### 2.2.2. $\varphi$>45°

When the observation site is at a high latitude, the maximum slope of the tangent to the $T_0$ contour line is less than 1. The analysis process is as follows:

First, obtain the maximum and minimum DEC degree on the $T_0$ contour line from

$$\sin T_0 = \sin\phi \sin DEC + \cos\phi \cos HA \cos DEC, \quad (18)$$

$$DEC_{\max} = 90° - \varphi, \quad (19)$$

and

$$DEC_{\min} = \varphi - 90°. \quad (20)$$

In Fig. 6, set the latitude of the observation site $\phi$ as 55°, the horizontal limit stop $T_0$ as 0°, and the altitude threshold of the observable sky area $T_1$ as 10°. Furthermore, $DEC_{\min}$ and $DEC_{\max}$ split the diagram into three regions. There are four possibilities to discuss according to which region the current telescope position $P_1(P_{1H}, P_{1D})$ and the target position $P_3(P_{3H}, P_{3D})$ belong to.

When $P_1 \in A$ and $P_3 \in A$, both $P_{1D}$ and $P_{3D}$ are greater than $DEC_{\max}$. Regardless of where $P_1$ and $P_3$ are located in region A, the pointing process will never traverse the region below the horizontal limit stop (see Fig. 7).

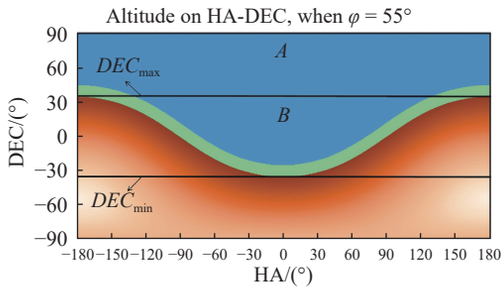


**Fig. 6. HA-DEC diagram divided by $DEC_{\min}$ and $DEC_{\max}$ on the $T_0$ contour line.**

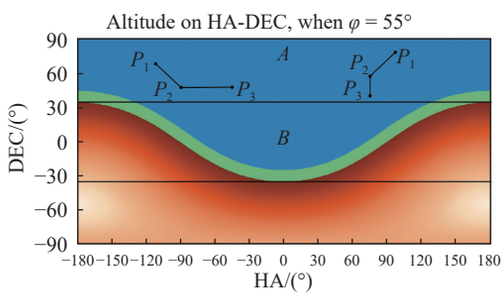


**Fig. 7. Two different types of pointing process trajectories when $P_1 \in A$ and $P_3 \in A$.**

For the case where $P_1 \in A$ and $P_3 \in B$, there are seven possibilities for the pointing process (see Fig. 8), which are the permutations and combinations of $P_{1H} > P_{3H}$, $P_{1H} < P_{3H}$, $P_{1H} = P_{3H}$ with $|P_{1H} - P_{3H}| > |P_{1D} - P_{3D}|$, and $|P_{1H} - P_{3H}| < |P_{1D} - P_{3D}|$. $P_2$, the turning point between dual-axis and single-axis pointing, is what determines whether the horizontal limit stop will be triggered or not. In the case of $|P_{1H} - P_{3H}| > |P_{1D} - P_{3D}|$, if the $P_2$ point is below the horizontal limit stop, the limit stop will occur, and will not otherwise.

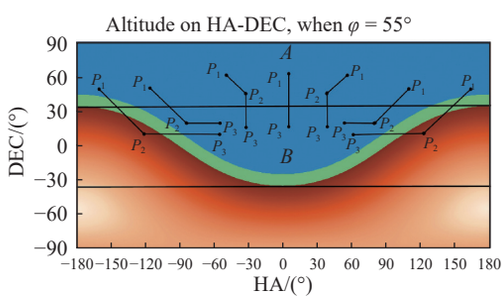


**Fig. 8. Seven different types of pointing process when $P_1 \in A$ and $P_3 \in B$.**

When $P_1 \in B$ and $P_3 \in A$, there are five possibilities for the pointing process (see Fig. 9), which are the permutations and combinations of $P_{1H} > P_{3H}$, $P_{1H} < P_{3H}$, $P_{1H} = P_{3H}$ with $|P_{1H} - P_{3H}| > |P_{1D} - P_{3D}|$, and $|P_{1H} - P_{3H}| < |P_{1D} - P_{3D}|$. In all typical cases, the turning points $P_2$ are all above the horizontal limit stop, so the pointing process will never pass through the region below the horizon.

Finally, when both $P_1 \in B$ and $P_3 \in B$, there are also

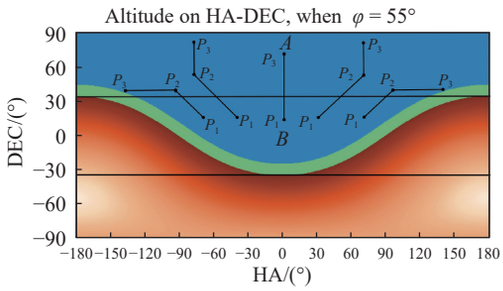


**Fig. 9. Five different types of pointing process when $P_1 \in B$ and $P_3 \in A$.**

seven possibilities of the pointing process (see Fig. 10). Similarly to the second case, $P_1 \in A$ and $P_3 \in B$, if the $P_2$ point is below the horizontal limit stop, the limit stop will occur, and will not otherwise.

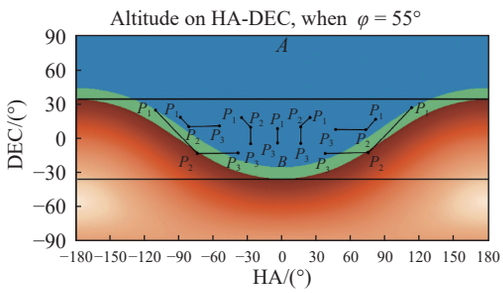


**Fig. 10. Seven different types of pointing process when $P_1 \in B$ and $P_3 \in B$.**

In summary, when the observation site is at a latitude higher than 45°, it is the turning point $P_2$ that determines whether the limit stop will trigger or not. If $P_2$ is below the horizontal limit stop, it will trigger, and it will not otherwise.

The coordinates of $P_2$ can be acquired with Equation (9)–Equation (16), and the altitude of $P_2$, to compare with the threshold $T_0$, can be calculated as

$$\sin ALT_{P_2} = \sin(P_{2D})\sin(\varphi) + \cos(P_{2D})\cos(P_{2H})\cos(\varphi). \tag{21}$$

## 3. AVOIDANCE ALGORITHM

After the prediction procedures, if the current pointing process is found to trigger the horizontal limit stop, the avoidance algorithm should be adopted to modify the pointing process, avoiding the limit stop. As shown in Fig. 11, when the original pointing process $P_1$–$P_2$–$P_3$ will trigger the limit stop, there are two methods to prevent it: modifying the turning point or altering the maximum pointing speed of one axis.

The pointing process of $P_1$–$P'_2$–$P_3$ alters the original order of dual-axis and single-axis process. At the first stage, the DEC axis is fixed, while the right ascension axis slews to the turning point $P'_2$. Subsequently, both axes rotate to the target position $P_3$. The location of $P'_2$ decides the duration of dual-axis motion, which also determines the duration of the overall pointing process. We choose the location of $P'_2$ to be symmetric with $P_2$. This path $P_1$–$P'_2$–$P_3$ does not prolong the duration of the pointing process and the courses are as simply as the original one. The coordination of $P'_2(P'_{2H}, P'_{2D})$ can be got from Equation (22) to (25). This method can be easily integrated with the telescope control software.

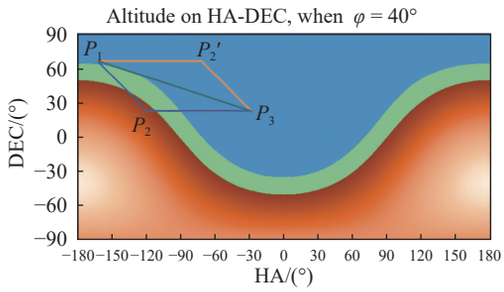


**Fig. 11. There are two ways to avoid the limit stop for the original $P_1$–$P_2$–$P_3$ process. When correctly slowing down the pointing velocity along the DEC axis, the path will be a straight line $P_1$–$P_3$. If the turning point is changed to to $P_2$', the pointing process will be $P_1$–$P_2$'–$P_3$.**

When $P_{1H} < P_{3H}$,

$$P'_{2D} = P_{1D}, \tag{22}$$

$$P'_{2H} = (P_{3D} - P_{1D}) + P_{3H}. \tag{23}$$

When $P_{1H} > P_{3H}$,

$$P'_{2D} = P_{1D}, \tag{24}$$

$$P'_{2H} = (P_{1D} - P_{3D}) + P_{3H}. \tag{25}$$

The other method is slowing down the pointing velocity of one axis. The maximum pointing speed generally cannot be increased because of safety considerations. To get the same pointing process duration as the original, the two axes should reach $P_3$ simultaneously. The altered trajectory on the chart is shown as the straight line $P_1 - P_3$. However, it cannot be guaranteed that the pointing process will completely avoid the horizontal limit stop in every case. Compared with altering speed, the method of changing the turning point is strongly preferred.

## 4. WORKFLOW FOR HORIZONTAL LIMIT STOP PREDICTION AND AVOIDANCE

We have created the workflow shown in Fig. 12 to demonstrate how to estimate and avoid the horizontal limit stop before every pointing process for an equatorial telescope. Assuming that the observation site is at the northern hemisphere, i.e. $\varphi > 0°$, the current position of the telescope axes is $P_1(P_{1H}, P_{1D})$, the target position is $P_3(P_{3H}, P_{3D})$, the horizontal limit stop is $T_0$, the lower alti-

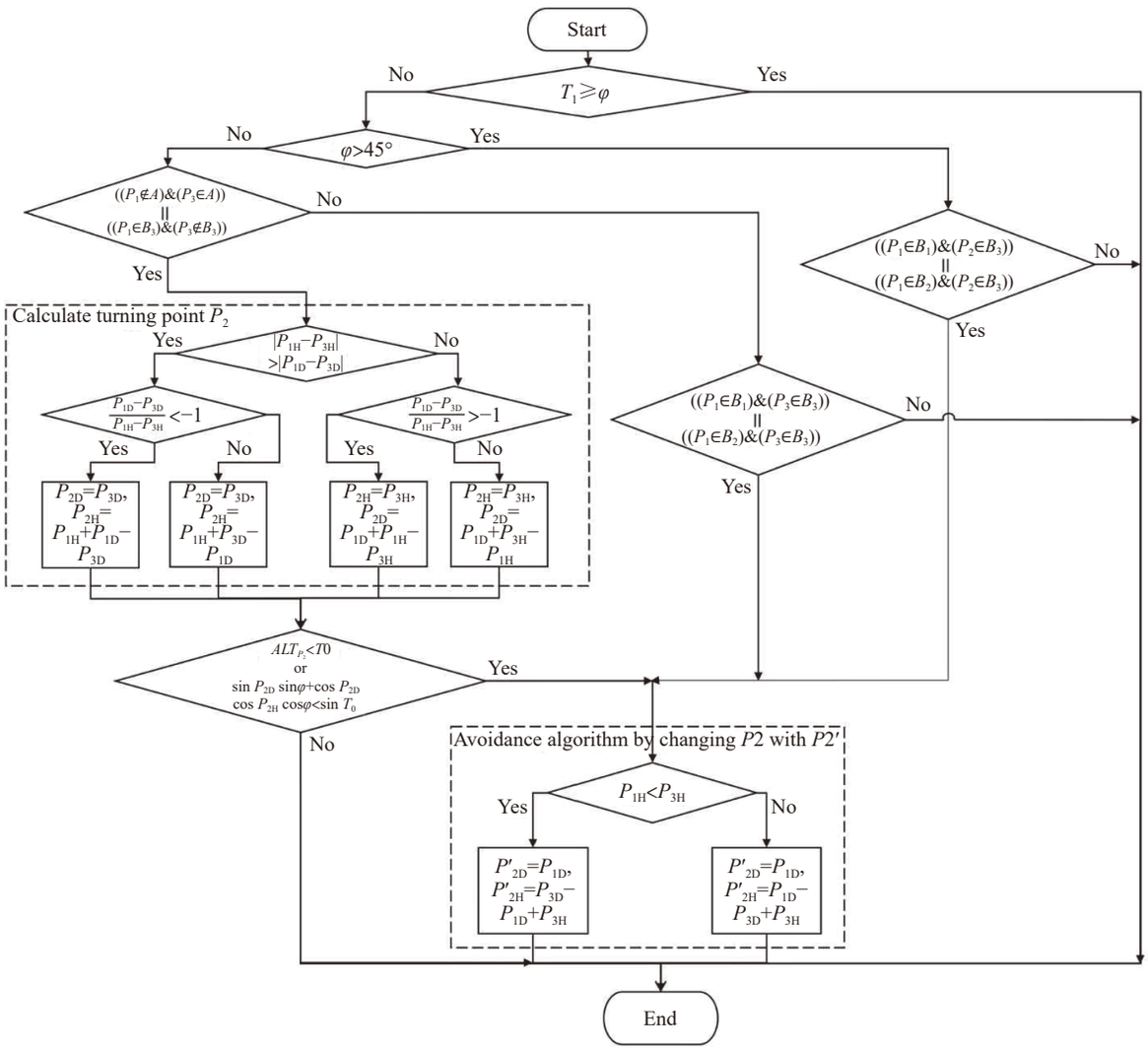


**Fig. 12. Flowchart of the prediction and avoidance algorithm.**

tude threshold of the observable sky area is $T_1$ ($T_1 > T_0$), and the maximum pointing speed and acceleration of the two axes of the telescope are the same.

## 5. EXTENDED DISCUSSION

### 5.1. Different Maximum Pointing Speed for the Two Axes

When the maximum pointing speeds of the two axes are not equal, the ratio of the maximum pointing speeds of the DEC and right ascension axis is set as $k$. The procedures we have determined require adjustment to account for this speed ratio.

Regarding the latitude threshold in Sections 2.2.1 and 2.2.2, our method differs from the previous approach as the trajectory of the telescope during the pointing process becomes a line segment with a slope approximately equal to $k$ or $-k$, rather than 1 or −1. Consequently, the analysis method described in Section 2.2 should be modified to examine whether the maximum slope of the $T_0$ contour exceeds $k$ instead of 1.

$P_2$ coordination can be acquired using Equation (26)–Equation (33):

When $|P_{1H} - P_{3H}| > |P_{1D} - P_{3D}|$ and $\frac{P_{1D} - P_{3D}}{P_{1H} - P_{3H}} < -k$:

$$P_{2D} = P_{3D}, \tag{26}$$

$$P_{2H} = \frac{1}{k}(P_{1D} - P_{3D}) + P_{1H}. \tag{27}$$

When $|P_{1H} - P_{3H}| < |P_{1D} - P_{3D}|$ and $\frac{P_{1D} - P_{3D}}{P_{1H} - P_{3H}} > -k$:

$$P_{2H} = P_{3H}, \tag{28}$$

$$P_{2D} = k(P_{1H} - P_{3H}) + P_{1D}. \tag{29}$$

When $|P_{1H} - P_{3H}| > |P_{1D} - P_{3D}|$ and $\frac{P_{1D} - P_{3D}}{P_{1H} - P_{3H}} < k$:

$$P_{2D} = P_{3D}, \tag{30}$$

$$P_{2H} = \frac{1}{k}(P_{3D} - P_{1D}) + P_{1H}. \quad (31)$$

When $|P_{1H} - P_{3H}| < |P_{1D} - P_{3D}|$ and $\frac{P_{1D} - P_{3D}}{P_{1H} - P_{3H}} > k$:

$$P_{2H} = P_{3H}, \quad (32)$$

$$P_{2D} = k(P_{3H} - P_{1H}) + P_{1D}. \quad (33)$$

For the intersection point $C$ and tangent line discussed in Section 2.2, the approach should be modified to accommodate the slopes of $k$ and $-k$ on the $T_0$ contour line accordingly. The equation for the altered turning point, $P'_2$, in the avoidance algorithm is also modified.

When $P_{1H} < P_{3H}$:

$$P'_{2D} = P_{1D}, \quad (34)$$

$$P'_{2H} = \frac{1}{k}(P_{3D} - P_{1D}) + P_{3H}. \quad (35)$$

When $P_{1H} > P_{3H}$:

$$P_{2D}{}' = P_{1D}, \quad (36)$$

$$P'_{2H} = \frac{1}{k}(P_{1D} - P_{3D}) + P_{3H}. \quad (37)$$

### 5.2. Pointing Process with Acceleration and Deceleration

To simplify, in the discussion above, we neglect acceleration and deceleration for the two axes. If we take this into account, there will be a minor difference in the movement trajectory at the starting point and the turning point, compared with that under the current assumption. The difference caused by this factor can be resolved with a sufficient intermediate zone, which is a region between the horizontal limit stop and the observable sky area, as is shown as the belt between $T_0$ and $T_1$. For a maximum pointing speed of the telescope, $V$, with a maximum acceleration of $a$, the maximum angular error caused by acceleration and deceleration is $V^2/2a$. Therefore, it is strongly recommended that the intermediate zone is larger than the maximum angular error. This can be expressed as

$$T_1 - T_0 > \frac{V^2}{2a}. \quad (38)$$

### 5.3. Observation Sites in the Southern Hemisphere

When the observation site is located in the Southern Hemisphere, the latitude $\varphi$ has a negative value. In this case, by reversing the direction of the declination axis on the HA-DEC plane chart and using the absolute value of the latitude for threshold comparisons, the resulting chart becomes identical to that of the Northern Hemisphere. Consequently, the algorithmic procedures described above can be directly applied to Southern Hemisphere sites without further modification.

## 6. CONCLUSION

To meet the observatory requirements of rapid response for observation of transient events and uninterrupted operation of telescopes, we discuss the issue of horizontal limit stops that may occur in equatorial telescopes during the pointing process. Using a plane-geometry based method, we investigate a procedure for predicting whether the horizontal limit stop will be triggered, and detail an avoidance algorithm for preventing the limit stop. The method can be used by a telescope control system to resolve this problem, and can help to guarantee that automatic and autonomous observations operate continuously, to provide a rapid response system for time-domain survey telescopes.


## ACKNOWLEDGEMENTS

This work was supported by National Key R&D Program of China (2023YFA1608300 and 2022YFC2807300).


## AI DISCLOSURE STATEMENT

AI-assisted technology is not used in the preparation of this work.

## AUTHOR CONTRIBUTIONS

Xiaoyan Li initiated this study, led the discussions, drafted the preliminary version of the paper and modified the manuscript. Yuling Cai derived the equations, conducted most of the analysis, and drafted the paper. Yuling Cai proposed the prediction and avoidance algorithms, and Xiaoyan Li refined them. Yanbing Chen contributed to the preliminary diagrams. All authors read and approved the final manuscript.

## DECLARATION OF INTERESTS

The authors declare no competing interests.

### REFERENCES


[1] Hu, Q., Yao, Z. 2006. Astronomical telescope design. Beijing: China Science and Technology Press. (in Chinese)

[2] Bely, P. Y. 2015. The design and construction of large optical telescopes. Beijing: Tsinghua University Press. (in Chinese)

[3] Cheng, J. Q. 2003. The principles of astronomical telescope design. Beijing: China Science and Technology Press. (in Chinese)

[4] Wu, X. X., Yang, H. B., Zhang, J. X., et al. 2009. Optical

design of support system for the large aperture sphere mirror. *Acta Photonica Sinica*, **38**(1): 129−132. (in Chinese)
[5] Wang, Y., Zhang, J. X., Yang, F. 2006. Support structure of large-aperture telescope primary mirror. *Infrared and Laser Engineering*, (Suppl 2): 31−34. (in Chinese)
[6] Li, X. Y., Jiang, F. H. 2023. A thresholding controllable horizontal limit trigger device for equatorial telescopes. CN219285499U. (in Chinese)
[7] Fan, Z., Sheng, Z. X., Li, Z., et al. 2023. Introduction of the SiTian Project. *Qinghai Science and Technology*, **30**(2): 18−28. (in Chinese)
[8] Meng, K. L., Sun, T. R., Hu, L., et al. 2022. Lenghu Astronomical Site Monitoring and Pilot Scientific Rsearch for Mega-science Facilities-Progress in the Pilot Scientific Research in Time-domain Astronomy. *Qinghai Science and Technology*, **29**(4): 25−42. (in Chinese)
[9] Fan, Y. F., Xin, Y. X., Bai, J. M., et al. 2015. An overview of the BOOTES-4 at the Lijiang Observatory. *Astronomical Research and Technology*, **12**(1): 78−88. (in Chinese)
[10] Albiac, F., Kalton, N. J. 2006. Topics in banach space theory. New York: Springer New York.